Quantification of abdominal aortic aneurysm wall enhancement with dynamic contrast-enhanced MRI : feasibility, reproducibility and initial experience

Please check the document version of this publication:

• A submitted manuscript is the version of the article upon submission and before peer-review. There can be important differences between the submitted version and the official published version of record. People interested in the research are advised to contact the author for the final version of the publication, or visit the DOI to the publisher's website.
• The final author version and the galley proof are versions of the publication after peer review.
• The final published version features the final layout of the paper including the volume, issue and page numbers.
[Link to publication](#)

Original Research

Quantification of Abdominal Aortic Aneurysm Wall Enhancement With Dynamic Contrast-Enhanced MRI: Feasibility, Reproducibility, and Initial Experience

V. Lai Nguyen, MD,[1,2]* Walter H. Backes, PhD,[2,3] M. Eline Kooi, PhD,[2,3]
Mirthe C.J. Wishaupt, BS,[1,2] Femke A.M.V.I. Hellenthal, MD, PhD,[1,2]
E. Marielle H. Bosboom, PhD,[4] Rob J. van der Geest, PhD,[5]
Geert Willem H. Schurink, MD, PhD,[1,2,6] and Tim Leiner, MD, PhD[2,7]

Purpose: To investigate the feasibility and reproducibility of dynamic contrast-enhanced MRI (DCE-MRI) to quantify abdominal aortic aneurysm (AAA) vessel wall enhancement dynamics which may reflect the amount of wall microvasculature. AAA vessel wall microvasculature has been linked with aneurysm progression and rupture.

Materials and Methods: Thirty patients with AAA underwent DCE-MRI at 1.5 Tesla. Enhancement dynamics of the aneurysm wall were quantified in regions-of-interest (ROIs) in the vessel wall by calculating the transfer constant (K^{trans}) using pharmacokinetic modeling and the area-under-gadolinium-curve (AUC). To assess reproducibility, 10 patients were imaged twice on different occasions. ROIs were drawn by two independent observers. The intraclass correlation coefficients (ICC) and coefficients of variation (CV) were determined to investigate intra-, interobserver, and interscan variability.

Results: Twenty-eight analyzable MR examinations were included for pharmacokinetic analysis after excluding two examinations due to severe motion artifacts. Intra-, inter-

observer, and interscan variability for K^{trans} were small (all ICC > 0.90, CV < 14%) as well as for AUC measurements (all ICC > 0.88, CV < 23%).

Conclusion: Quantitative analysis of AAA vessel wall enhancement dynamics with DCE-MRI is feasible and reproducible.

Key Words: dynamic contrast-enhanced MRI; abdominal aortic aneurysm; microvascularization; vessel wall imaging
J. Magn. Reson. Imaging 2014;39:1449–1456.
© 2013 Wiley Periodicals, Inc.

IT IS GENERALLY accepted that abdominal aortic aneurysm (AAA) is a degenerative inflammatory disease of the aortic wall resulting in dilatation which, when left untreated, will ultimately lead to rupture and death (1). To prevent rupture, AAA with a diameter larger than 55 mm are treated. However, diameter-guided surgical intervention is not a perfect tool as small AAA can also rupture (2). Therefore, better biomarkers are required to predict AAA progression and rupture in individual patients.

Recent insights from histological studies suggest that increased microvasculature of the AAA vessel wall plays a pivotal role in aneurysm progression and rupture (3–5). Once formed, microvasculature of the vessel wall is a relevant source of inflammatory cells and matrix metalloproteinases (MMPs) that induce breakdown of the extracellular matrix, which results in vessel wall strength loss (6).

In the past decade, it has been shown that dynamic contrast-enhanced MRI (DCE-MRI) is able to quantify microvasculature of the vessel wall in carotid arterial occlusive disease (7,8). Pharmacokinetic modeling of DCE-MRI enables quantification of the transfer constant K^{trans}, which reflects microvascular flow, permeability, and surface area. Therefore it is expected that a vessel wall with large K^{trans} values is more prone to

the entrance of inflammatory cells and MMPs into the vessel wall. The application of this technique to study microvasculature in the AAA vessel wall has not yet been demonstrated so far. The aim of the present study was, therefore, to investigate the feasibility and reproducibility of DCE-MRI to quantify AAA vessel wall enhancement dynamics. To this end, the rate of vessel wall enhancement expressed by K^{trans} and area-under-curve (AUC), were studied. The AUC represents the area under concentration time curve and it has been shown that this parameter could serve as a model-free measures for quantification of microvessel density (9,10).

MATERIALS AND METHODS

Subjects

From January 2010 to May 2011 consecutive patients with known AAA (maximal diameter > 3.0 cm) were invited to participate in the present study. Exclusion criteria were presence of contraindications for MRI and/or severely impaired renal function (estimated glomerular filtration rate [eGFR] $\leq$ 30 mL/min/1.73 m^2). In total, 30 patients were included and underwent MRI examinations. The local Medical Ethics Committee approved the study and all patients provided written informed consent before inclusion. Permission was given to image 10 subjects twice to investigate interstudy reproducibility.

MRI Protocol

A schematic representation of the MRI protocol is given in Figure 1. Patients were imaged on a 1.5 Tesla (T) whole body MRI system (Intera, Philips Healthcare, Best, The Netherlands) using the standard four-channel body coil. MRI acquisition parameters are listed in Table 1. In all patients, dynamic series of 25 T1-weighted (T1w) fast-field echo (FFE) images were acquired at each of five different levels of the aneurysm. A sequential two-dimensional single-slice acquisition was used with full sampling of one slice before sampling the next slice. The time interval between two images was approximately 18 s. The most proximal slice was positioned at the neck of the AAA and the middle slice was positioned at the maximal diameter of the aneurysm. Image acquisition was performed using electrocardiographic gating (gate delay, 295 ms; gate width, 376 ms). As the dynamic scan duration per dynamic phase was approximately 18 seconds, approximately 15–25 cardiac phases were averaged. During acquisition of the dynamic series 0.1 mmol/kg body weight gadobutrol (Gadovist 1.0 mmol/mL, Bayer Schering Pharma Ag, Berlin, Germany) contrast agent was injected in the antecubital vein at a rate of 0.5 mL/s with a power injector (Medrad Spectris, Indianola, PA). The injection was performed coincidently with the start of the sixth scan of the dynamic series.

After the acquisition of the dynamic series, T1w three-dimensional turbo field echo (TFE) anatomical images were acquired. The acquisition of the T1w TFE
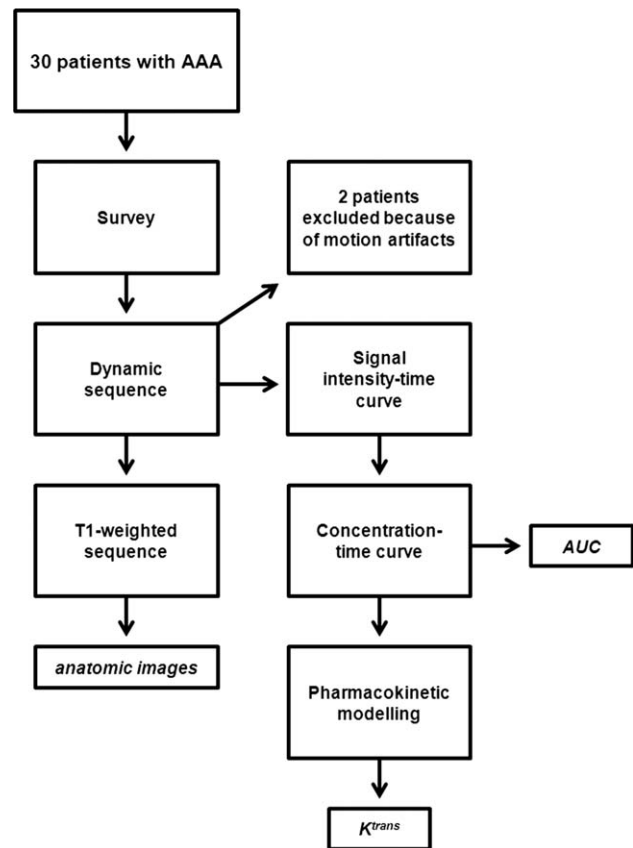
Figure 1. A schematic representation of the MRI protocol.

images was carried out approximately 8 min after contrast injection. The MRI sequence parameters are listed in Table 1.

The first 10 consecutive patients who provided informed consent for a second examination underwent this MRI examination with a mean period of 7 days (range, 6–9 days) between scans with exactly the same MRI-protocol to assess interscan variability to investigate the extent of physiologic, scanning, and data analysis variations. Distance to the aortic bifurcation and specific points on the vertebral column were used as landmarks for spatial co-registration of the two examinations.

Image Analysis

The AAA vessel wall was identified on the T1w TFE anatomical images and regions-of-interest (ROI) around the inner and outer vessel wall boundaries were drawn using a custom-made image analysis package (Vessel MASS). ROIs were carefully drawn to not include other structures other than the AAA vessel wall. For this purpose, images were zoomed in the postprocessing software until segmentation was possible. Nevertheless, we cannot completely rule out partial volume effects. Subsequently, the Vessel-MASS software automatically copied the ROIs to the dynamic images using multi-planar reformation. Before kinetic analysis, the ROIs in all images were checked and if necessary ROIs were redrawn to correct for any displacements. All ROIs were drawn at

Table 1
Acquisition Parameters for MRI Measurements

Parameter	DCE- MRI TRF	DCE-MRI[a] AIF	T1-w TFE Anatomy
Scan mode	Multi2D	Multi2D	3D
Technique	FFE	FFE	TFE
TR (ms)	13.0	19.0	15.0
TE (ms)	1.50	1.50	1.00
Flip angle (°)	35°	35°	15°
FOV (mm)	400	380	380
Voxel dimensions (acquired) (mm)	$1.58 \times 1.58 \times 6.00$	$3.96 \times 3.96 \times 6.00$	$1.04 \times 1.49 \times 1.50$
Voxel dimensions (reconstructed) (mm)	$0.79 \times 0.79 \times 6.00$	$1.48 \times 1.50 \times 6.00$	$0.79 \times 0.79 \times 1.50$
No. of slices	5	5	52[b]
No. of dynamic phases	25	108	–
Temporal resolution (s)	18[c]	5[c]	–
Fat suppression	No	No	Yes
Scan direction	Axial	Axial	Axial
Scan duration (min:s)	8:00[d]	8:00[d]	6:30[b]

[a]A cranial spatial saturation slab was applied to suppress blood signal before contrast agent arrival.
[b]The number of slices, and therefore scan duration, varied from subject to subject, depending on the dimensions of the AAA.
[c]The temporal resolution of the scans was dependent on the subjects' heart rate.
[d]Scan duration was dependent on subjects' heart rates.

the level of the maximal diameter in aneurysms with a layer of intraluminal thrombus. Presence of a concentric thrombus with a minimal thickness of two pixels at the thinnest part of the thrombus was required to avoid partial volume artifacts due to inclusion of vessel lumen into wall ROI. To investigate the association of DCE-MRI parameters with thrombus thickness, additional ROIs were drawn around the vessel lumen boundaries to determine thrombus thickness at the level of the maximal diameter.

To investigate the interobserver agreement, the ROIs were drawn independently by two observers. To assess intraobserver agreement Observer 1 drew the ROIs twice. Possible recall bias between the first and second session for Observer 1 was minimized by analyzing the blinded images with an interval of 4 weeks and randomization of the order of the images. For interscan agreement testing, Observer 1 performed the same image analysis for the second MRI examination of the 10 patients imaged twice.

Pharmacokinetic Measures

The pharmacokinetic model as described by Patlak et al (11) was used to quantify contrast agent dynamics from the DCE images. For this purpose a custom-made Matlab (Mathworks, Natick, MA) program was used to calculate the pharmacokinetic measures using the following equation, which describes the temporal changes in contrast agent concentrations:

$$C_t(t) = v_p \cdot C_p(t) + K_{trans} \cdot \int_0^t C_p(\tau)d\tau$$

Here, $C_t(t)$ is the contrast concentration time-course in vessel wall tissue, $C_p(t)$ is the concentration in blood plasma, v_p is the fractional blood plasma volume and K^{trans} is the uni-directional transfer constant that quantifies the rate of vessel wall enhancement corrected for the arterial supply of contrast agent. In this two-compartment model any reflux of contrast

medium from the extravascular extracellular space (v_e) back to the blood space is neglected (ie, k = $K^{trans}/v_e \cong 0$). The motivation of this simplified model is that no reflux of the contrast agent in tissue enhancement curves was observed in the acquisition time window of 8 min and the extension of the model by a reflux constant k provided relatively large uncertainties in the additional parameter (k or v_e) and no improvements of the fitted enhancement curves. In other words, the impulse response function is represented by a step function or a very slowly decaying exponential function exp(−k·t), of which the reflux rate k is very slow with respect to the acquisition window to observe the decay. Considering the dynamic scan interval of approximately 18 s, the onset times of tissue enhancement and contrast agent arrival for the arterial input function were taken to be equal.

Concentration (C_t)-time-courses were derived from the signal intensity time courses using the Ernst equation (12), the known r_1 and r_2 relaxivities and fixed values for precontrast T_1 and T_2 relaxation times of 900 ms and 30 ms, respectively .

C_p time-courses were derived from the contrast-enhanced image signal intensity time courses determined from arterial blood. This measure is also known as the arterial input function (AIF). In this study, we used a generalized AIF that was derived from data in three additional patients with AAA that underwent dynamic contrast-enhanced MR imaging with high temporal resolution (interval of 5 seconds between two dynamic images). MRI acquisition parameters are listed in Table 1. The AIFs were determined from a circular ROI positioned at the center of the aortic lumen where flow artifacts are minimal. Once C_t and C_p are determined, the pharmacokinetic measure K^{trans} and v_p can be computed by a nonlinear least-square optimization algorithm. In the present study, the measure v_p was not further analyzed in detail.

K^{trans} was determined in a voxel-wise manner. The mean K^{trans}-value was computed by averaging over all vessel wall voxels per slice. In addition, the
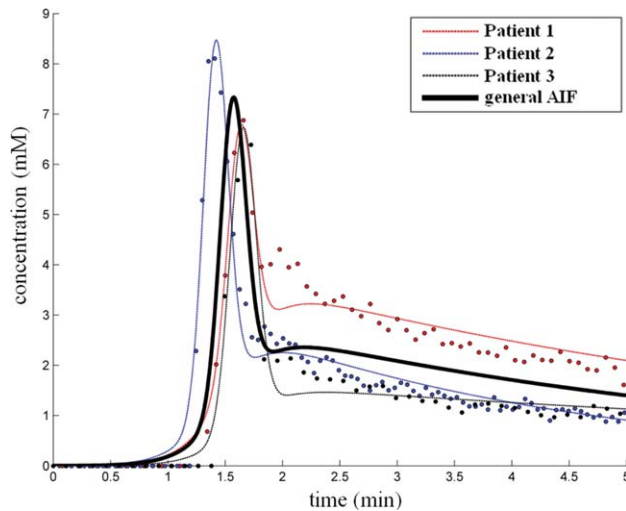
Figure 2. General arterial input function (thick black line) derived from three individual concentration time-courses and fits of the data from a ROI in the aorta lumen.

area-under-curve (AUC) was determined by calculating the integral of the tissue residue function over two time intervals: 1 and 5 min from the onset of enhancement.

Statistical Analysis

The interscan, intra-, and interobserver variability of K^{trans} and AUC were expressed in terms of the intraclass correlation coefficients (ICC) with 95% confidence intervals and the coefficient of variation (CV in %). The CV was calculated by dividing the overall mean within-subject standard deviation by the mean measurement value over all subjects. To visualize variabilities, Bland-Altman plots were constructed. Correlations between K^{trans}, AUC, and maximal diameter as well as thrombus thickness were investigated using the Pearson correlation coefficient (r). All statistical tests were performed with the statistical software package SPSS 18.0 (SPSS Inc., Chicago, IL); P values below 0.05 were considered significant.

RESULTS

Two of the 30 examinations were excluded from analysis because of extensive motion artifacts. This was caused by patient movement and respiratory artifacts. Therefore the success rate was 93% (28/30 subjects). The remaining examinations from 28 patients (mean age $\pm$ SD: 72 $\pm$ 6.1 years; M/F: 24/4) with an AAA maximal diameter of 49.6 $\pm$ 5.8 mm (mean $\pm$ SD) were included for pharmacokinetic analyses.

The AIFs could be determined properly with the dedicated high temporal resolution DCE-MRI protocol. The general AIF averaged over the three subjects is shown in Figure 2 and served as a patient-independent input to the pharmacokinetic analysis. The vessel wall could be identified in all included examinations. MRI signal time series acquired from the 28 patients could be converted into concentration over time and fitted successfully using the pharmacokinetic model. An example of AAA vessel wall enhancement and identification as well as successful fitting of the concentration time course from one representative patient are shown in Figure 3. The resulting K^{trans} map from this patient is also included.

The intra-, interobserver, and interscan variability were small, as evidenced by high ICCs for K^{trans} and AUC (Table 2). This is also visualized in the Bland-
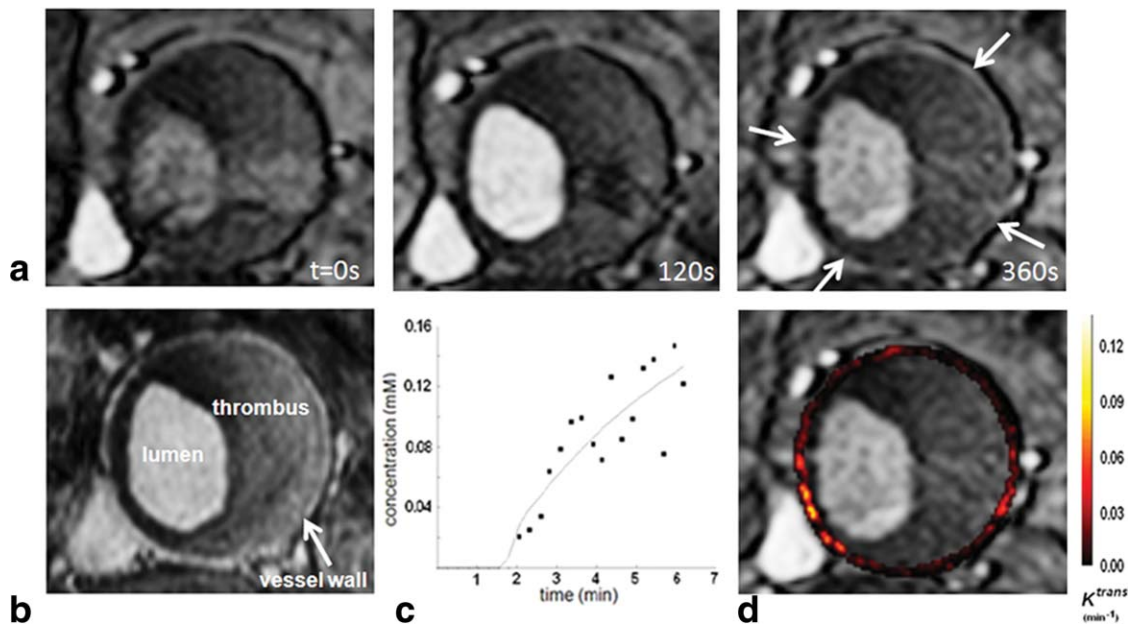
Figure 3. Vessel wall enhancement and identification from one representative patient. **a:** Three of the 25 images from a dynamic series at different time points. Contrast arrived at the aneurysm lumen at t = 120 s. Vessel wall enhancement (indicated by white arrows) is visible at t = 360 s. **b:** T1w TFE anatomical image. The vessel wall is clearly visible. **c:** Contrast agent time course of the vessel wall from all pixels and fit of the time course data (black line) using the pharmacokinetic model. **d:** K^{trans} map showing distribution of K^{trans} values throughout the vessel wall.

Table 2

K^{trans} and AUC Intra-, Interobserver and Interscan Variability

	K^{trans} (min^{-1})	AUC (1min) (mM*min)	AUC (5min) (mM*min)
Intraobserver			
Scan 1 (Session 1, Observer 1)	0.024 (0.01)	0.143 (0.08)	0.341 (0.17)
Scan 1 (Session 2, Observer 1)	0.025 (0.01)	0.151 (0.08)	0.354 (0.17)
CV (%)	7.9	12.7	10.7
ICC	0.96	0.97	0.96
Interobserver			
Scan 1 (Observer 1)	0.024 (0.01)	0.143 (0.08)	0.341 (0.17)
Scan 1 (Observer 2)	0.023 (0.01)	0.127 (0.06)	0.302 (0.19)
CV (%)	13.9	11.9	10.4
ICC	0.93	0.89	0.91
Interscan			
Scan 1 (Observer 1, n = 10)	0.024 (0.01)	0.135 (0.09)	0.329 (0.19)
Scan 2 (Observer 1, n = 10)	0.027 (0.01)	0.170 (0.11)	0.408 (0.22)
CV (%)	12.7	22.2	19.6
ICC	0.92	0.90	0.93

Standard deviations are indicated in parentheses.

Altman plots (Fig. 4). The intersubject variations for K^{trans} and AUC were much larger than the interscan variation. No systematic differences were found in the variabilities of K^{trans} or AUC between the three sources of variation. For K^{trans}, the ICC was highest for intraobserver variability (ICC = 0.96) and lowest for the interscan variability (ICC = 0.92). The range between the 95% agreement lines was narrowest for intraobserver variability and widest for the interscan variability. Figure 4c shows a trend of higher K^{trans} variability for higher mean K^{trans} values. All CV for K^{trans} were lower than 14%. To illustrate interscan reproducibility, MR images with K^{trans} maps overlay from one patient examined 1 week apart are shown in Figure 5.

For the AUC, the CV was somewhat lower for AUC measured up to 5 min compared with AUC measured up to 1 min, for intra- and interobserver as well as interscan variability (Table 2). The highest CV (22.2%) was found for the interscan AUC at 1 min.

There was a strong positive correlation between K^{trans} and AUC 1 min (Pearson r = 0.74; P < 0.001) as well as AUC 5 min (r = 0.84; P < 0.001) (Fig. 6). A moderate positive correlation of r = 0.52 (P = 0.005) was found between AAA maximal diameter (mean ± SD: 49.6 ± 5.8 mm) and K^{trans}. For AUC, a relatively weak, nonsignificant positive correlation was found with AAA maximal diameter at 1 min (r = 0.27; P = 0.2), and a trend toward a moderate positive correlation was found at 5 min (r = 0.32; P = 0.09). A poor correlation was found between thrombus thickness (mean ± SD: 8.6 ± 4.8 mm) and K^{trans} (r = −0.11; P = 0.6). A trend toward a moderate negative correlation was found between thrombus thickness and AUC at 1 min (r = −0.36; P = 0.06) and AUC at 5 min (r = −0.37; P = 0.06).

DISCUSSION

In the present study, we investigated the feasibility and reproducibility of dynamic contrast-enhanced MRI to quantify enhancement dynamics related to AAA vessel wall microvasculature. We found DCE-MRI of the AAA wall to be a reproducible technique that can be used to investigate AAA vessel wall enhancement dynamics as expressed by the transfer constant K^{trans}, or the AUC in the vast majority of examined subjects. The technical success rate of the described protocol was high, and there was low intra- and interobserver as well as interscan variability. The intersubject variation for K^{trans} and AUC were much larger than the intrasubject variation indicating that the interscan variability is small enough to investigate intersubject differences in future studies. We also found that K^{trans} was only moderately correlated with the maximal diameter, suggesting that these two parameters are related but not interchangeable.
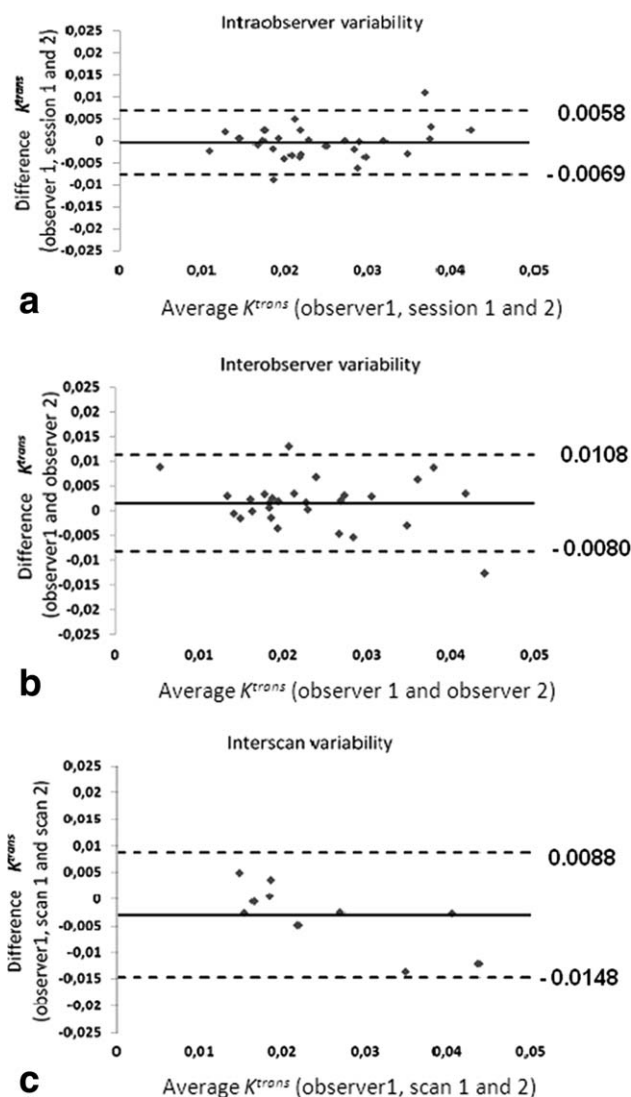

Figure 4. Bland-Altman plots for intra-, interobserver, and interscan variability for K^{trans} (a, b, and c, respectively). The lines represent the average difference while the limits of agreement (± 1.96 SDs) are drawn as dashed lines.
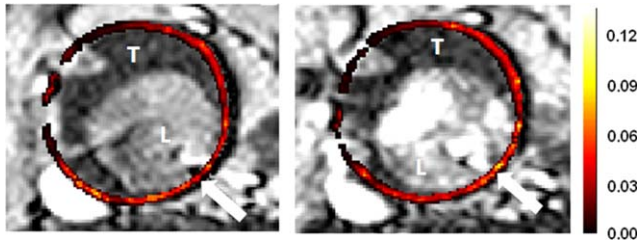
Figure 5. T1w MR images with K^{trans} maps overlay from one patient (maximal diameter of 53 mm). Images were acquired 1 week apart. White arrows indicate the vessel wall with K^{trans} map overlay (T = thrombus, L = lumen). The generated K^{trans} maps color scale (dark red represents low K^{trans} value) and the K^{trans} distribution for the two examinations are similar, but with a little mismatch in anatomic location between the first and second MRI scan which was unavoidable. [Color figure can be viewed in the online issue, which is available at wileyonlinelibrary.com.]

Note that the reproducibility assessment involves variations in the day-to-day physiologic status of the patients' vessel wall, variations in MR scanning (e.g., slice positioning), and variations in data analysis (e.g., drawing of ROI). However, variations in arterial input function were not included. For this study, we used a generalized arterial input function averaged over several patients, which thus ignores day-to-day variations in patients and differences between patients. Due to the DCE-MRI protocol used in this study, it was not possible to determine individual AIF and TRF in one examination because of inaccuracies in precise determination of peak arterial enhancement with the temporal resolution used. A high temporal resolution (AIF) scan before the scan to investigate AAA vessel wall enhancement is possible but impractical for clinical use and might moreover affect the vessel enhancement of the next scan by contrast agent retention.

A higher temporal resolution scan may increase K^{trans} estimation precision but comes at the cost of reduced spatial resolution, which may lead to errors in K^{trans} estimate due to partial volume effects of the AAA vessel wall. The temporal resolution of the dynamic scans in this study is comparable with former studies investigating vessel wall enhancement in carotid arterial occlusive disease which has been shown to quantify the amount of plaque microvasculature (13). In contrary to carotid studies, it was necessary to use a much larger field of view to investigate the abdominal aorta. It should be mentioned that the temporal resolution of the scans was also dependent

on the subjects' heart rate because image acquisition was performed using electrocardiographic gating. This may have somewhat contributed to the interscan variabilities. A small mismatch may have occurred between the first and second MRI scan, which may have induced higher coefficient of variation values. However, the small interobserver variabilities were mainly caused by the differences in applying the correction for small incoherencies between the anatomical T1w images and the dynamic images. Above all, the low intra-, interobserver, and interscan variabilities indicate that the MRI protocol used is suitable to investigate AAA vessel wall enhancement.

To optimize kinetic analysis, we used a slow injection rate (0.5 mL/s), which weakens the requirement of high temporal resolution and thus provides a possibility to increase the spatial resolution. Previously, Aerts et al (14) showed that a higher injection rate is most beneficial for high values of K^{trans} (> 0.2 min^{-1}), but for low values (< 0.2 min^{-1}) the errors in K^{trans} estimation are much smaller and the injection rate is less critical. This also explains to some extent the higher interscan K^{trans} variability in AAA patients with the highest K^{trans} values. By applying a relatively low injection rate, T2* signal decay artifacts during the peak concentration and undersampling artifacts of a sharp bolus are avoided, which are more likely occurring for a high injection rate.

Walker-Samuel et al (15) showed that AUC is a mixed parameter and found a positive correlation with K^{trans}. In this study, we also found a strong positive correlation between K^{trans} and AUC. Because AUC is a model-free and robust measure for vessel wall microvasculature (8,10), this may suggest that the K^{trans} values found in the present study are reliable. Histological studies will have to show which parameter best corresponds with the actual amount of AAA vessel wall microvessels. However, AUC as a parameter has the disadvantage that it reflects a combination of various mechanisms mediating contrast agent concentration thus complicating the interpretation of a specific physiological change. In addition, no significant correlation between AUC and maximal diameter, which is the current standard for rupture risk, were found.

It has been shown that intraluminal thrombus can alter AAA wall inflammation and wall stress acting on the vessel wall (16,17). However, the exact mechanism remains unclear. In the present study, we found no clear relationship between thrombus thickness and
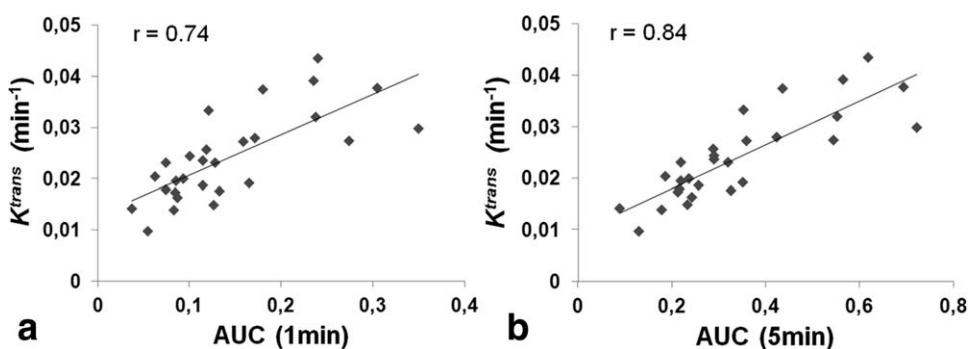

Figure 6. a: Correlation between AUC (1 min) and K^{trans} (Pearson r = 0.74; $P < 0.001$). **b:** Correlation between AUC (5min) and K^{trans} (r = 0.84; $P < 0.001$).

AUC. Also, no significant correlation was found between thrombus thickness and K^{trans}. The tendency for a moderate negative correlation between thrombus thickness and AUC might be explained by a protective effect of a thicker layer of thrombus to circulatory stress on the vessel wall (18,19). On the other hand, others have suggested that thrombus present in AAA may also serve as a proinflammatory stimulus on AAA vessel wall inflammation by secreting proteolytic enzymes (20,21). However, the relation between thrombus size and the amount of proinflammatory stimulus remains unclear because most of the inflammatory activity is only found at the luminal part of the thrombus.

A limitation of the present study is that there was no reference standard to which we could compare the pharmacokinetic parameters. This study lacks histological quantification of AAA vessel wall microvasculature, which is necessary for the validation of the technique. As the included patients had relatively small AAAs, not all patients were candidates for surgical treatment. It remains to be determined whether K^{trans} accurately reflects the amount of AAA vessel wall microvasculature. A second limitation is that only AAA with a layer of intraluminal thrombus with a minimal thickness of two pixels were included. Because there was no noticeable enhancement of mural thrombus after contrast injection, there was no interference with assessment of the vessel wall on contrast-enhanced MR images. Because of this requirement and the absence of thrombus in normal abdominal aorta, this work is solely limited to the diseased aorta. Third, v_p values for the aortic wall were found to be very low and therefore could not be determined accurately. It is most likely that v_p values will not improve the stratification of AAA severity. Future studies at higher field strengths might improve v_p estimation. Finally, a limitation is that fixed precontrast T_1 and T_2 relaxation times were used for conversion of vessel wall signal intensity into concentration for all patients. We chose this approach because high spatial resolution T_1 mapping of the vessel wall was impractical in a clinical setting due to time and signal-to-noise constraints.

MRI has previously been used to investigate AAA vessel wall inflammation and whether it can stratify AAA with a high expansion rate (22). It was shown that AAA with distinct uptake of ultrasmall superparamagnetic particles of iron oxide (USPIO) by vessel wall macrophages grow faster. However, the USPIO agent (Sinerem, Guerbet) used in that study is, however, no longer commercially available. DCE-MRI is an interesting alternative because it has been demonstrated that this technique can both quantify the amount of vessel wall macrophages and microvascularization in atherosclerotic carotid plaques within one scan session (23). Furthermore, future studies should investigate whether there is a relationship between AAA vessel wall enhancement dynamics and thrombus inflammatory composition as well as high peak wall stress, which are considered risk factors for rapid AAA progression and rupture (24–26). The results from these studies may provide valuable insights in the pathophysiology involved in the evolution of AAA and severity of the disease in individual patients.

In conclusion, the results of the present study showed that DCE-MRI can be used to quantitatively analyze AAA vessel wall enhancement dynamics with low intra-, interobserver, and interscan variabilities. Prospective studies are warranted to elucidate the potential of DCE-MRI to stratify AAA that are prone to rapid expansion and rupture. Furthermore, its applicability to evaluate medical therapies intending to prevent AAA related future adverse events can be explored.

REFERENCES

1. Koch AE, Haines GK, Rizzo RJ, et al. Human abdominal aortic aneurysms. Immunophenotypic analysis suggesting an immune-mediated response. Am J Pathol 1990;137:1199–1213.
2. Nicholls SC, Gardner JB, Meissner MH, Johansen HK. Rupture in small abdominal aortic aneurysms. J Vasc Surg 1998;28:884–888.
3. Choke E, Thompson MM, Dawson J, et al. Abdominal aortic aneurysm rupture is associated with increased medial neovascularization and overexpression of proangiogenic cytokines. Arterioscler Thromb Vasc Biol 2006;26:2077–2082.
4. Holmes DR, Liao S, Parks WC, Thompson RW. Medial neovascularization in abdominal aortic aneurysms: a histopathologic marker of aneurysmal degeneration with pathophysiologic implications. J Vasc Surg 1995;21:761–771; discussion 771–762.
5. Paik DC, Fu C, Bhattacharya J, Tilson MD. Ongoing angiogenesis in blood vessels of the abdominal aortic aneurysm. Exp Mol Med 2004;36:524–533.
6. Reeps C, Pelisek J, Seidl S, et al. Inflammatory infiltrates and neovessels are relevant sources of MMPs in abdominal aortic aneurysm wall. Pathobiology 2009;76:243–252.
7. Kerwin W, Hooker A, Spilker M, et al. Quantitative magnetic resonance imaging analysis of neovasculature volume in carotid atherosclerotic plaque. Circulation 2003;107:851–856.
8. Calcagno C, Cornily JC, Hyafil F, et al. Detection of neovessels in atherosclerotic plaques of rabbits using dynamic contrast enhanced MRI and 18F-FDG PET. Arterioscler Thromb Vasc Biol 2008;28:1311–1317.
9. Cheng HL, Chen J, Babyn PS, Farhat WA. Dynamic Gd-DTPA enhanced MRI as a surrogate marker of angiogenesis in tissue-engineered bladder constructs: a feasibility study in rabbits. J Magn Reson Imaging 2005;21:415–423.
10. Calcagno C, Vucic E, Mani V, Goldschlager G, Fayad ZA. Reproducibility of black blood dynamic contrast-enhanced magnetic resonance imaging in aortic plaques of atherosclerotic rabbits. J Magn Reson Imaging 2010;32:191–198.
11. Patlak CS, Blasberg RG, Fenstermacher JD. Graphical evaluation of blood-to-brain transfer constants from multiple-time uptake data. J Cereb Blood Flow Metab 1983;3:1–7.
12. Ernst RR. Application of Fourier transform spectroscopy to magnetic resonance. Rev Sci Instrum 1966;37:93.
13. Kerwin WS, O'Brien KD, Ferguson MS, Polissar N, Hatsukami TS, Yuan C. Inflammation in carotid atherosclerotic plaque: a dynamic contrast-enhanced MR imaging study. Radiology 2006;241:459–468.
14. Aerts HJ, van Riel NA, Backes WH. System identification theory in pharmacokinetic modeling of dynamic contrast-enhanced MRI: influence of contrast injection. Magn Reson Med 2008;59:1111–1119.
15. Walker-Samuel S, Leach MO, Collins DJ. Evaluation of response to treatment using DCE-MRI: the relationship between initial area under the gadolinium curve (IAUGC) and quantitative pharmacokinetic analysis. Phys Med Biol 2006;51:3593–3602.
16. Vorp DA, Lee PC, Wang DH, et al. Association of intraluminal thrombus in abdominal aortic aneurysm with local hypoxia and wall weakening. J Vasc Surg 2001;34:291–299.
17. Koole D, Zandvoort HJ, Schoneveld A, et al. Intraluminal abdominal aortic aneurysm thrombus is associated with disruption of wall integrity. J Vasc Surg 2012;57:77–83.
18. Wang DH, Makaroun MS, Webster MW, Vorp DA. Effect of intraluminal thrombus on wall stress in patient-specific models of abdominal aortic aneurysm. J Vasc Surg 2002;36:598–604.

19. Georgakarakos E, Ioannou CV, Volanis S, Papaharilaou Y, Ekaterinaris J, Katsamouris AN. The influence of intraluminal thrombus on abdominal aortic aneurysm wall stress. Int Angiol 2009;28:325–333.

20. Fontaine V, Jacob MP, Houard X, et al. Involvement of the mural thrombus as a site of protease release and activation in human aortic aneurysms. Am J Pathol 2002;161:1701–1710.

21. Coutard M, Touat Z, Houard X, Leclercq A, Michel JB. Thrombus versus wall biological activities in experimental aortic aneurysms. J Vasc Res 2010;47:355–366.

22. Richards JM, Semple SI, MacGillivray TJ, et al. Abdominal aortic aneurysm growth predicted by uptake of ultrasmall superparamagnetic particles of iron oxide: a pilot study. Circ Cardiovasc Imaging 2011;4:274–281.

23. Kerwin WS, Oikawa M, Yuan C, Jarvik GP, Hatsukami TS. MR imaging of adventitial vasa vasorum in carotid atherosclerosis. Magn Reson Med 2008;59:507–514.

24. Kazi M, Thyberg J, Religa P, et al. Influence of intraluminal thrombus on structural and cellular composition of abdominal aortic aneurysm wall. J Vasc Surg 2003;38:1283–1292.

25. Fillinger MF, Marra SP, Raghavan ML, Kennedy FE. Prediction of rupture risk in abdominal aortic aneurysm during observation: wall stress versus diameter. J Vasc Surg 2003;37:724–732.

26. Di Martino ES, Vorp DA. Effect of variation in intraluminal thrombus constitutive properties on abdominal aortic aneurysm wall stress. Ann Biomed Eng 2003;31:804–809.